Chapter 6

Taguchi optimization and ANN modeling for Uni-array Vortex Generators

Overview: The present chapter investigates the thermohydraulic performance of different vortex generator (VG) geometries in a rectangular channel under varying ambient conditions. The examined VG shapes include delta (D), envelope (M), and fishtail (F), with ambient heat transfer coefficients (HTCs) of 5, 15, and 25W/m²K. Various thermal and fluid flow parameters are considered to evaluate performance. The study employs the Taguchi design of experiments to determine the necessary run combinations, while analysis of variance (ANOVA) and signal-to-noise (S/N) ratios help identify the optimal factors influencing the outcome. Additionally, an artificial neural network (ANN) model is developed, demonstrating high prediction accuracy with a strong coefficient of determination.

6.1 Geometry, Governing Equation, and Boundary Conditions

The arrangement of the vortex generators has been shown in Fig. 6.1 (a-c). The vortex generators shown are (a) Delta VG (DVG), (b) Envelope VG (MVG, the acronym M for their M-like shape), and Fishtail VG (FVG). The dimensions of the channel under study are 360mm x 70mm x 20mm (length x width x height). The angle of inclination (θ) employed here is 60° respectively, as per the findings of the previous chapter. Thus, a total of 8 VGs are placed inside the rectangular channel. The distance between consecutive VGs is 40mm. The angle of inclination (θ) is defined as the angle between the face of the vortex generator and the horizontal as depicted in Fig. 6.2 (a). Fig. 6.2 (b-d) exhibits the geometry of the different vortex generators used.

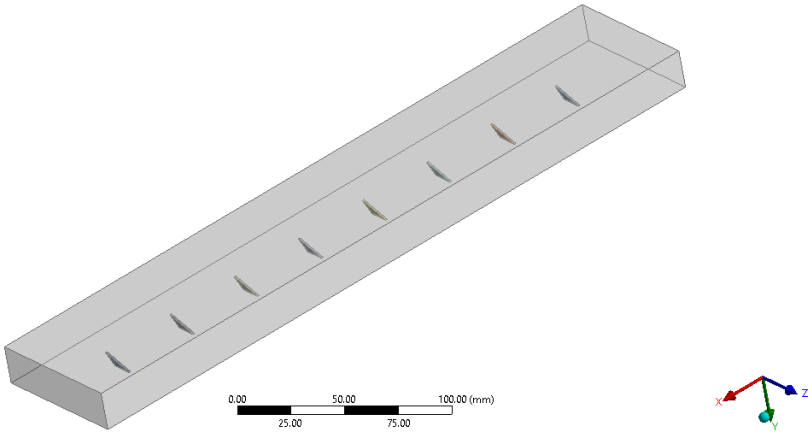

(a)

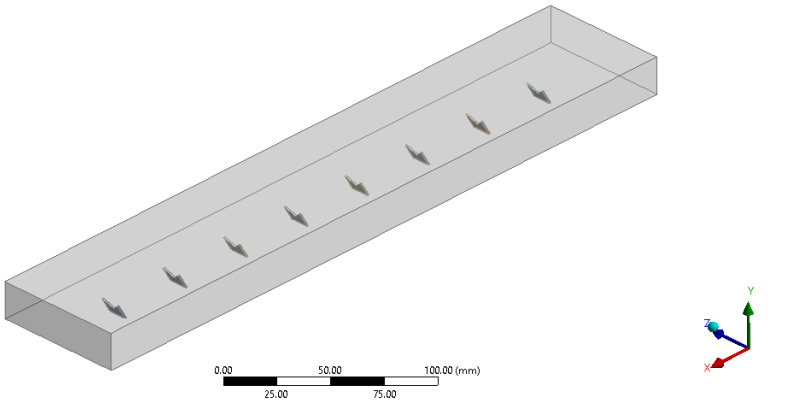

(b)

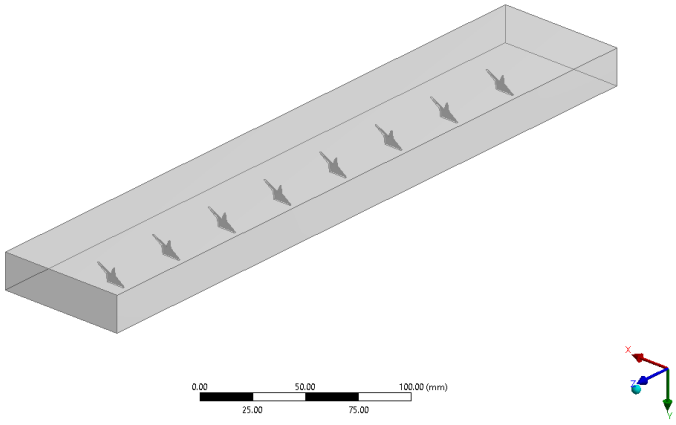

(c)

Fig. 6.1 (a-c) Different Vortex Generator configurations

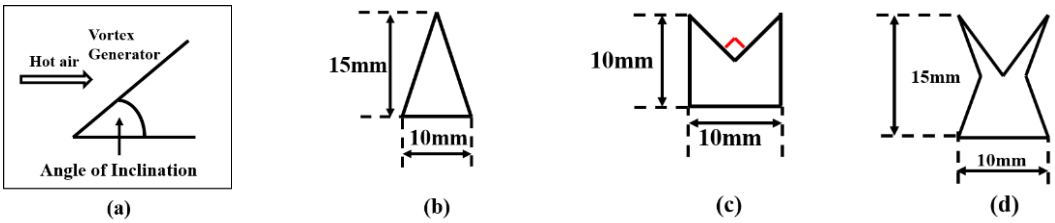

Fig. 6.2 (a) Angle of inclination definition, (b-d) Dimensions of the VGs

When the hot air flows past these vortex generators, their path gets deflected and vortices are formed. Vortex generators create controlled vortices or swirls in the fluid flow. This increased turbulence disrupts the boundary layer, promoting better mixing among the fluid particles. Enhanced turbulence results in more efficient heat transfer by diminishing the thickness of the thermal boundary layer and upsurging the heat transfer coefficient. A low-pressure region is created just adjacent to the vortex generators. This causes whirling of the hot air, which mixes the fluid thoroughly. The growth of the thermal boundary layer is disrupted. However, it also increases turbulence in the flow. Turbulence causes more frictional losses as the fluid moves through the channel, resulting in a higher pressure drop. The vortices themselves also dissipate energy as they interact with the fluid, further contributing to pressure loss. Furthermore, different shapes of the VGs produce different flow patterns, resulting in unique hydraulic and thermal performances. Several vortex generators in an array help to enhance the thermal action by continuously disrupting the flow. The numerical analysis has been done using ANSYS 2022R2.

In this study, the considered hot air is treated as incompressible and continuous, and the simulations are conducted under stable states. The determination of the heat exchanger surface temperature is achieved through the application of conjugate heat transfer equations within the computational unit. The governing eqs. are as follows:

Continuity Eq., $\frac{\partial}{\partial x_i}(\rho u_i) = 0$ (6.1)

Momentum Eq., $\frac{\partial}{\partial x_i}(\rho u_i u_k) = \frac{\partial}{\partial x_i}\left(\mu \frac{\partial u_k}{\partial x_i}\right) - \frac{\partial p}{\partial x_k}$ (6.2)

Energy Eq., $\frac{\partial}{\partial x_i}(\rho u_i T) = \frac{\partial}{\partial x_i}\left(\Gamma \frac{\partial T}{\partial x_i}\right)$ (6.3)

Here, ρ and μ represent density and dynamic viscosity, respectively. The diffusion coefficient Γ is defined as thermal conductivity divided by the specific heat ($\Gamma=k/Cp$). Eqs. (6.4) and (6.5) simulate turbulent flow using the k-ε model, as given by (Wilcox, 1998).

$$\frac{\partial}{\partial x_i}(\rho k u_i) = \frac{\partial}{\partial x_j}\left[\left(\mu + \frac{\mu_t}{\sigma_k}\right)\frac{\partial k}{\partial x_j}\right] + G_k + G_b - \rho\epsilon - Y_M + S_k \tag{6.4}$$

$$\frac{\partial}{\partial x_i}(\rho \epsilon u_i) = \frac{\partial}{\partial x_j}\left[\left(\mu + \frac{\mu_t}{\sigma_\epsilon}\right)\frac{\partial \epsilon}{\partial x_j}\right] + C_{1\epsilon}\frac{\epsilon}{k}(G_k + C_{3\epsilon}G_b) - C_{2\epsilon}\rho\frac{\epsilon^2}{k} + S_\epsilon \tag{6.5}$$

Within this framework, G_k, G_b, and Y_M signify the creation of turbulence kinetic energy arising from the mean velocity gradient, buoyancy effects, and the involvement of fluctuating dilation in turbulence towards the comprehensive dissipation rate. The constants $C_{1\epsilon}$, $C_{2\epsilon}$, and $C_{3\epsilon}$ play a crucial role in these formulations. The turbulent viscosity, μ_t, is modeled as:

$$\mu_t = \rho C_\mu \frac{k^2}{\epsilon} \tag{6.6}$$

The production of k is defined by the following Eqs.:

$$P_k = -\rho \overline{u_i' u_j'} \frac{\partial u_j}{\partial x_i} \tag{6.7}$$

$$P_k = \mu_t S^2 \tag{6.8}$$

Where the mean rate of strain tensor, S, is:

$$S \equiv \sqrt{2 S_{ij} S_{ij}} \tag{6.9}$$

The channel is supplied with a uniform velocity and temperature of the hot air at the inlet. No-slip boundary condition prevails at the walls. The rectangular channel is subjected to natural convection in the surroundings. Boundary conditions are specified at the inlet, and wall as follows:

Inlet: $u = u_{in}, v = w = 0, T = T_{in}$ (6.10)

Wall: $u = v = w = 0, q = q_{conv}$ (6.11)

The heat conservation eq. can be derived for each control volume, delineating the heat dissipation within the control unit originating from the hot gas (Q).

$$Q_i = m_e C_{p,e}(T_{e,i} - T_{e,i+1}) \tag{6.12}$$

The average control unit temperature can be computed utilizing Eq. (6.13). Furthermore, convective heat transfer is given by Eq. (6.14).

$$T_{avg\ i,i+1} = \frac{T_{e,i} + T_{e,i+1}}{2} \tag{6.13}$$

$$Q_i = h_{e,i} Ar\left(T_{avgi,i+1} - T_{in,i,i+1}\right) \tag{6.14}$$

The friction factor and TEF are determined using the Eqs. (6.15), and (6.16) respectively.

$$f = \frac{(\Delta P/L) D_m}{(\rho V^2/2)} \tag{6.15}$$

$$TEF = \frac{\frac{Nu}{Nu_o}}{\left(\frac{f}{f_o}\right)^{1/3}} \tag{6.16}$$

Here, *Nu* is the Nusselt number, Nu_o is for a smooth channel, *f* is the friction factor, and f_{or} smooth channel.

6.2 Grid Independence Test and Data Validation

The comprehensive simulations conducted for 3D vortex generators on heat exchangers necessitate precise mesh generation to accurately compute temperature and

velocity distributions. Considering the complexity of VGs, a tetrahedral mesh is utilized for fluid and plate areas, while a quad-mesh is employed for upstream and downstream extended regions, as depicted in Figs. 6.3(a-c). An adaptive mesh refinement technique is applied to the fluid regions and the walls of VGs to ensure a finer mesh.

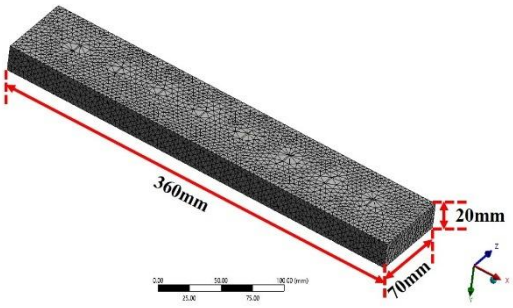

(a)

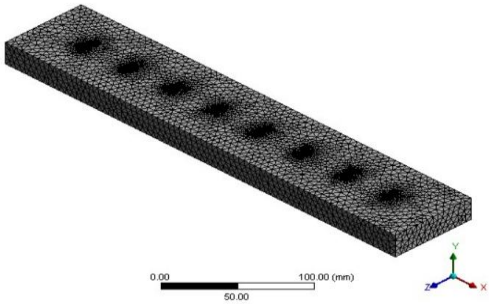

(b)

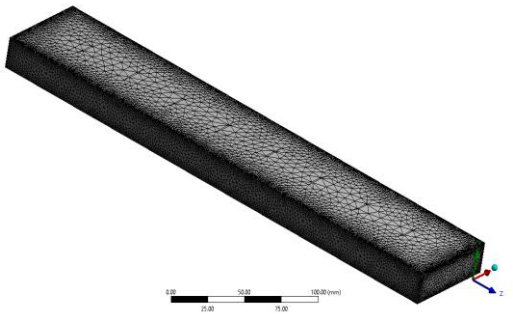

(c)

Fig. 6.3 (a-c) Meshing of VGs and rectangular channel

To evaluate numerical accuracy, flow through a channel with vortex generators set at a 60° angle, and fishtail-shaped at node 1, was studied. Four different grid

configurations, ranging from 104,003 to 853,102 elements, were examined. Table 6.1 illustrates that the grid setup containing 571,835 cells displays a comparative discrepancy in HTC and pressure drop of less than 1% compared to the configuration with the highest number of cells (853,102). Therefore, for subsequent calculations, the grid configuration with 571,835 cells or a closely resembling setup was selected as the working grid size, with consideration given to computational resources and computation time.

Table 6.1: Grid Independence Test (α=60°, distance to height=2, fishtail shape)

Grid	Elements	h(W/m^{2}K)	Error	ΔP(Pa)	Error
Grid 1	104,003	101.878	-	39.7574	-
Grid 2	324,866	98.1927	3.61%	35.7181	10.15%
Grid 3	571,835	95.8460	2.37%	34.4426	11.96%
Grid 4	853,102	96.0089	0.19%	34.6182	0.50%

Fig. 6.4 shows the data validation for the present study with the experimental work discussed previously. Validation has been performed for fishtail vortex generator configuration (α=60°, distance to height=2). The extreme discrepancy occurs at the highest Reynolds number. The validation is done for the smooth channel. The deviation value calculated reaches a maximum of 6.77%. The cause of this may be the presence of environmental conditions like ambient temperature variation during the experiment, humidity content in the air, and experimental uncertainties. The maximum deviation is well within the acceptable limits.

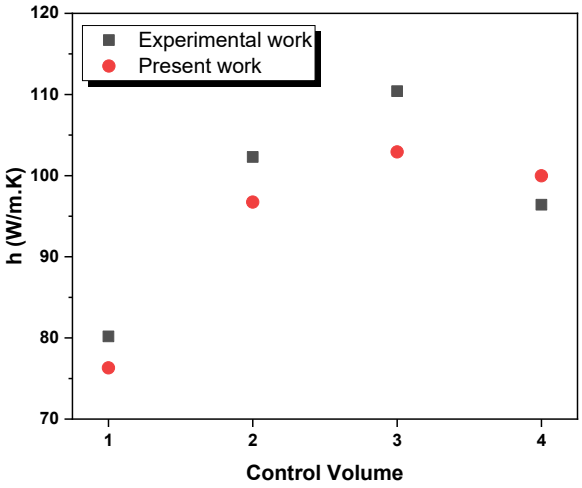

Fig. 6.4 Validation with experimental work

6.3 Taguchi's Analysis-Design of experiments

The Taguchi method is a statistical approach to optimization and quality improvement in processes. It aims to minimize variation and improve the quality of methods and processes by identifying and optimizing the influential factors (also called parameters or control factors) that affect method or process performance. The first step in the Taguchi method is to identify the key factors that influence the value of the product or process. Once the control factors are identified, the next step is to design a set of experiments to systematically study the effects of these factors on the response variable (the quality characteristic being optimized). The Taguchi method typically uses orthogonal arrays, which allow for a relatively small number of experiments to be conducted while still providing robust and reliable results. Orthogonal arrays are structured matrices that ensure a balanced and efficient allocation of experimental runs across the different combinations of control factors. The S/N ratio measures the deviation of the response variable from the target value relative to the variability in the process. After conducting the experiments and collecting the data, statistical analysis techniques are used to analyze the results and identify the optimal levels of the control factors that

minimize variation and maximize the S/N ratio. This often involves techniques such as analysis of variance (ANOVA) to determine the criticality of the factors and their interactions. In the current study, input factors and levels have been used to create Taguchi experiments using Minitab 16 software. Two factors namely, the shape of the VGs and the ambient condition, with three levels each are taken for optimizing output response. Fig. 6.5 and Table 6.2 depict the flowchart of Taguchi analysis, and input parameters along with their levels respectively.

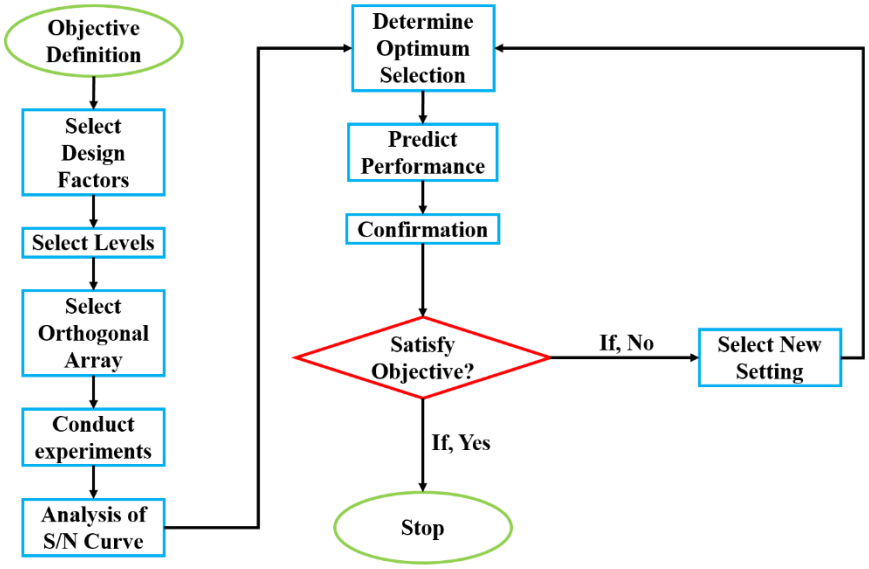

Fig. 6.5 Taguchi flowchart

Table 6.2: Input factors and levels for the Taguchi method

Factor	**Input Parameter**	**Levels**		
A	Shape of the VG	Delta	Envelope	Fishtail
B	Ambient HTC (W/m^2K)	5	15	25
Objective function	Thermal Enhancement Factor (TEF)			

In the present study, the output response is required to be as large as possible. Hence the criteria chosen here is larger is better. Under such circumstances, the following correlation is deployed:

$$\frac{S}{N}\text{HB} = -10\log\left(1/n\sum_{i=1}^{n}\frac{1}{Y_i^2}\right) \tag{6.17}$$

While the Reynolds number is a critical parameter for fluid flow, its well-established effects are extensively documented in prior research. Including it as a variable would redundantly increase the number of experimental runs and computational cost without providing novel insight. This study instead focuses its analysis on the less-explored, critical factors of vortex generator geometry and ambient heat transfer coefficient to efficiently isolate their unique impact on thermohydraulic performance.

6.4 Artificial Neural Network

In the present study, ANN has been employed using MATLAB 16 software. Artificial neural networks (ANNs) in MATLAB work by simulating the behavior of biological neural networks to solve various computational tasks, such as pattern recognition, classification, regression, and optimization. Leveraging its strength in discerning intricate patterns, the Artificial Neural Network (ANN) was employed to process the dataset through a structured pipeline. This involved training the model to recognize underlying relationships, validating its parameters to prevent overfitting, and finally testing its predictive accuracy on a separate subset of data to evaluate its generalization capability. A suitable ratio of training, validating, and testing data set is used to acquire the maximum value of the coefficient of determination (R^2), which represents better predictability of the ANN model.

6.5 Results and Discussion

6.5.1 Numerical Analysis

Figs. 6.6 (a-c) show the temperature profile for the delta, envelope, and fishtail VGs arranged in a uni-array manner in the rectangular channel. Figs. 6.6 (a-c) show profiles for vertical and horizontal midplanes. Vortex generators are observed to have a significant influence on the temperature of air flowing in a rectangular channel. By introducing vortices into the flow, the VGs enhance the heat transfer between the air and the channel walls. This is typically achieved by promoting better mixing of the air, which helps to diminish the boundary layer thickness and increase convection. As a result, the temperature of the air tends to decrease more rapidly as it moves through the channel, leading to improved thermal performance. Additionally, vortex generators can help to reduce flow separation. Furthermore, Figs. 6.7 (a-c) showcase the pressure profiles for the delta, envelope, and fishtail VGs arranged in a uni-array manner in the rectangular channel. Vortex generators tend to induce local pressure variations along with themselves, leading to changes in pressure distribution. From Figs. 6.7 (a-c), it is clear that the first VG creates a region of higher pressure drop. Moreover, they influence the overall pressure drop across the channel, primarily aiming to enhance flow mixing and heat transfer. However, their impact on pressure can vary; they may delay flow separation and reattachment, increase pressure losses, develop controlled airflow patterns, depending on the vortex generator geometry, and improve overall flow performance. Ultimately, the effect of VGs on air temperature and pressure in a rectangular channel is complex, influenced by factors like design, placement, and airflow characteristics. The temperature is predominantly uniform in the upper section of the channel (Figs. 6.8 (a-c)). The bottom region near the vortex generators shows slight temperature variations because the vortex generators induce localized mixing. Slight cooling effects are observed near the last

vortex generator (small blue/green region). This suggests an enhancement in heat transfer due to increased turbulence. Temperature reduction is subtle, implying that while the vortex generators enhance heat transfer, the flow is still dominated by the high-temperature inlet condition.

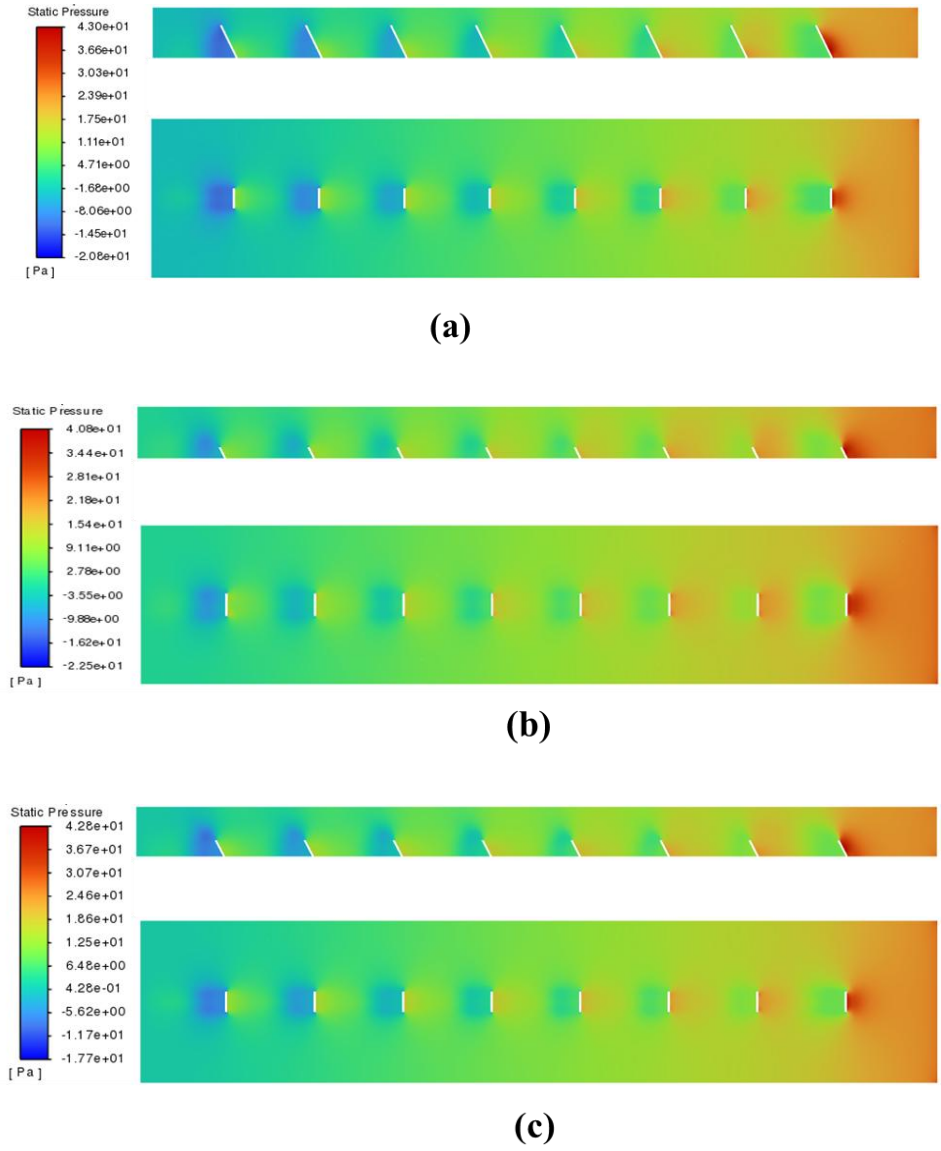

Fig. 6.6 Pressure contours for (a) Delta VG, (b) Envelope VG, and (c) Fishtail VG

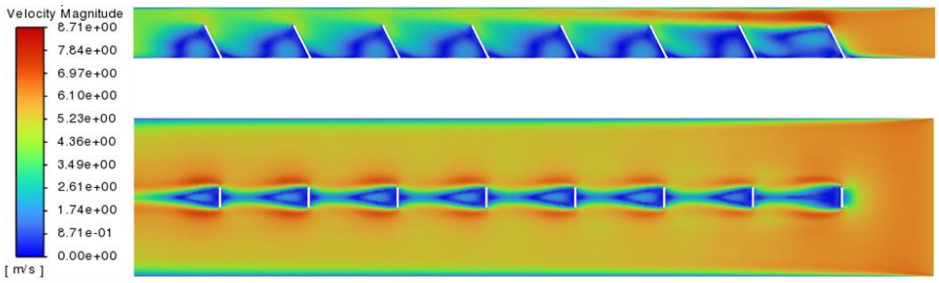

(a)

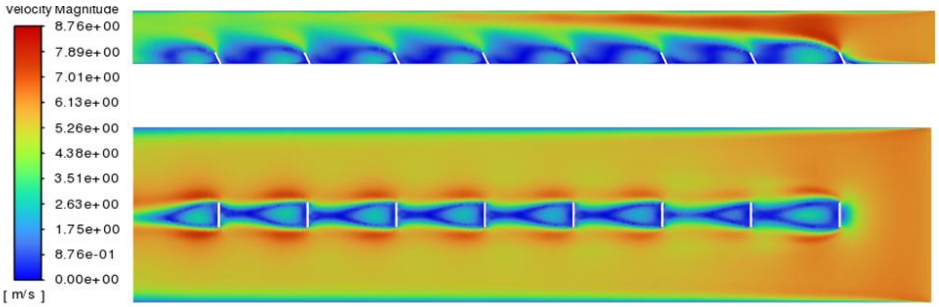

(b)

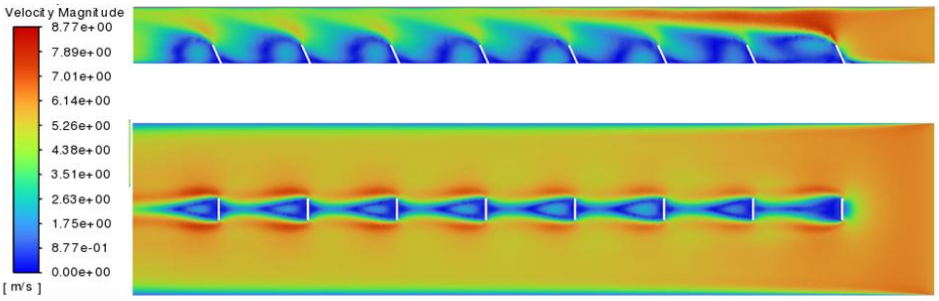

(c)

Fig. 6.7 Velocity contours for (a) Delta VG, (b) Envelope VG, and (c) Fishtail VG

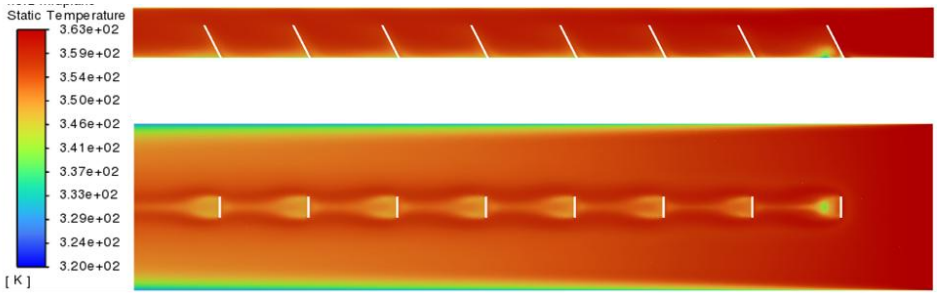

(a)

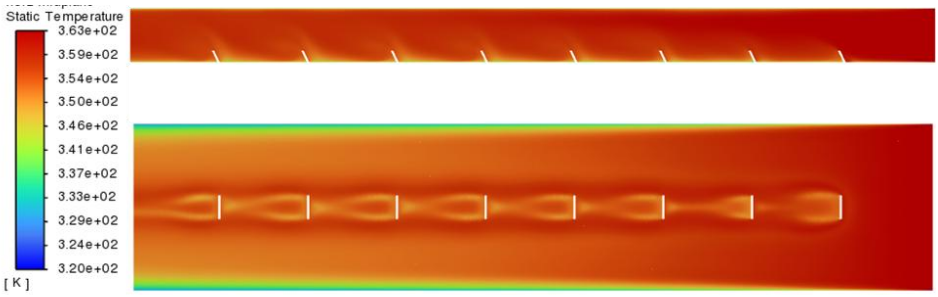

(b)

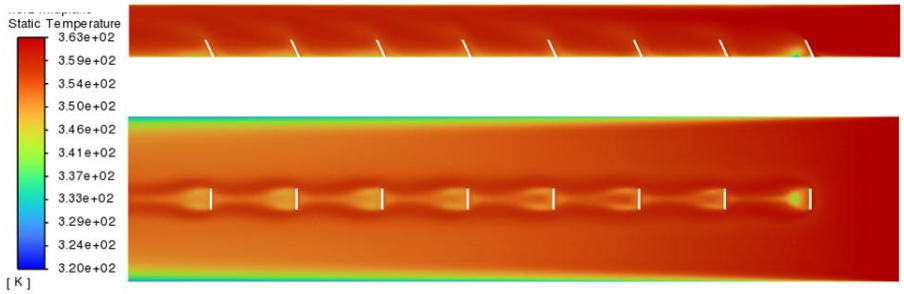

(c)

Fig. 6.8 Temperature contours for (a) Delta VG, (b) Envelope VG, and (c) Fishtail VG

6.5.2 Heat transfer capability

Figs. 6.9 (a-d) shows the variation of the heat transfer coefficient for different conditions. The impact of different ambient conditions (varying ambient HTC) has been studied in Figs. 6.9 (a-c). Three different configurations of VGs have been investigated for their heat transfer capabilities in comparison to that of a smooth rectangular channel. It is seen in Figs. 6.9 (a-c) that the HTC increases after every consecutive computational domain. For all the cases, the channels with VGs exhibit a higher value of *h* than the ones without the VGs. Quantitatively, the heat transfer coefficient value at the outlet increases by 2.797, 2.777, and 2.834 times for DVG, MVG, and FVG respectively as compared to the inlet for h=25W/m^{2}K. Similarly, for h=15W/m^{2}K, *h* raises by 2.801, 2.783, and 2.838 times at the outlet when compared to the parameter value at the inlet. For h=5W/m^{2}K, these values are 2.785, 2.766, and 2.566 for DVG, MVG, and FVG respectively. This

happens because, VGs enhance heat transfer by increasing turbulence, promoting mixing of fluid flow, and delaying boundary layer separation. Vortex generators introduce turbulence into the flow, which helps break up the boundary layer. Boundary layer separation can lead to reduced heat transfer efficiency as it creates stagnant regions where heat exchange is limited.

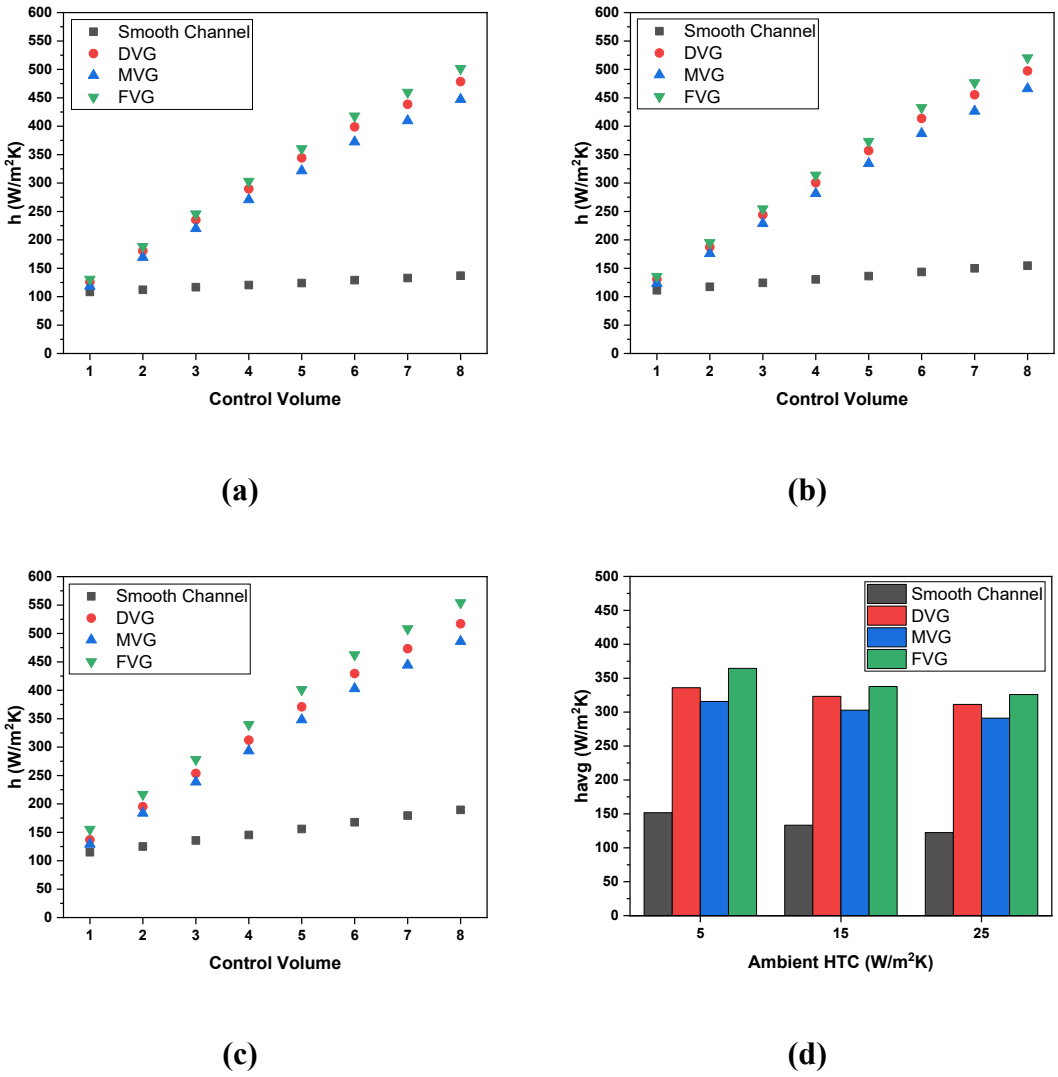

Fig. 6.9 Variation of (a) heat transfer coefficient in computational domains for h=25W/m²K, (b) h=15W/m²K, (c) h=5W/m²K and (d) Average heat transfer coefficient for different ambient conditions

By delaying separation, vortex generators ensure that the flow remains attached to the surface for longer, maximizing heat transfer. By increasing turbulence, promoting

mixing, and delaying boundary layer separation, vortex generators effectively increase the heat transfer coefficient. This means that for a given temperature difference between the fluid and the surface, more heat is transferred per unit area and per unit time. Out of all these, the maximum heat transfer coefficient is exhibited by FVG with a value of 554.17W/m^2K for h=5W/m^2K.

However, it is also observed that as the ambient heat transfer coefficient increases, the internal coefficients decrease, owing to the cooling effect of higher ambient heat transfer coefficients. This is evident from Figs. 8 (a-c). A higher ambient heat transfer coefficient causes greater heat dissipation and reduced external thermal resistance. The above fact is also evident from Fig. 6.9 (d) where a decrement in the average ***h*** is observed as the ambient heat transfer coefficient increases. It shows the variation of the average heat transfer coefficient for smooth channel, DVG, MVG, and FVG against different values of ambient heat transfer coefficient. The impact of ambient HTC can be observed here, for instance at h=25W/m^2K, 15W/m^2K, and 5W/m^2K, the average internal heat transfer coefficients for the smooth channel are 122.475W/m^2K, 133.4W/m^2K, and 151.687W/m^2K respectively. For h=25W/m^2K, the average HTC for DVG, MVG, and FVG incorporated channels are 154.26%, 137.7%, and 166.13% higher than that of the smooth channel. When the ambient condition is studied at h=15W/m^2K, this increment is found to be 142.28%, 127.07%, and 153.18% for DVG, MVG, and FVG respectively. Furthermore, the parameter value increases by 121.51%, 108.14%, and 140.33% for DVG, MVG, and FVG respectively, against the smooth channel for h=5W/m^2K. Thus, the vortex generators exhibit great heat transfer enhancement with their incorporation in the smooth channel. In summary, the decrease in the internal HTC when the external heat transfer coefficient increases is a consequence of the changing balance of thermal resistances within the system, with the reduction in external thermal resistance playing a

more significant role. Nevertheless, the maximum average HTC is shown by the Fishtail VG with a value of 501.57W/m^2K, 520.37W/m^2K, and 554.18W/m^2K for h=25W/m^2K, 15W/m^2K, and 5W/m^2K. Nevertheless, the results show that the internal HTC is sensitive to the VG shape and ambient conditions.

6.5.3 Impact on pressure drop

Fig. 6.10 depicts the manner of the pressure drop along the computational domains or length of the channel in smooth and DVG, MVG, and FVG-incorporated rectangular channels. It is seen from the Fig. that the pressure drop decreases along the length of the channel for all the configurations. The pressure drops by 84.94%, 92.42%, 91.39%, and 89.44% for the smooth-, DVG-, MVG-, and FVG-incorporated channels. Thus, higher pressure drop is observed in channels with vortex generators. This is because of increased turbulence, energy dissipation, boundary layer effect, flow obstruction, and development of secondary flow. Turbulence causes more frictional losses as the fluid moves through the channel, resulting in a higher pressure drop. The creation of vortices requires energy. This energy is taken from the flow, leading to a reduction in kinetic energy and an increase in pressure. The vortices themselves also dissipate energy as they interact with the fluid, further contributing to pressure loss. Furthermore, VGs disrupt the boundary layer of the fluid flowing over the channel walls. This disruption increases mixing and promotes heat transfer, but it also affects the flow profile and increases shear stresses at the channel walls. This results in higher frictional losses and consequently, a higher pressure drop along the channel. It is commendable that the change in ambient conditions does not affect the pressure drop. In quantitative terms, the highest pressure occurs for the DVG arrangement, followed by MVG, FVG, and the smooth channel. The smooth channel will have the least pressure drop due to the absence of any obstruction to the flow. The

maximum value of pressure drops exhibited by the smooth channel, DVG-, MVG-, and FVG- arrangements are 1.042Pa, 2.704Pa, 2.622Pa, and 2.533Pa.

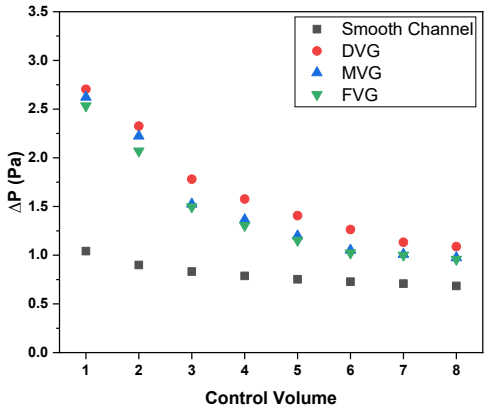

Fig. 6.10 Pressure drop variation along the channel

The reason for this observation can be understood with the help of Fig. 6.11. As seen from the diagram, DVG creates vortices all along its height, MVG creates vortices on the sides as well as the top V-notch, and FVG- also creates a vortex in the top V-notch region. Even though all their cross-section areas are the same, DVG possesses greater height than the MVG and hence its domain of influence increases. On the other hand, the side cuts of the FVG allow a smoother flow of the vortex generator when compared to the MVG.

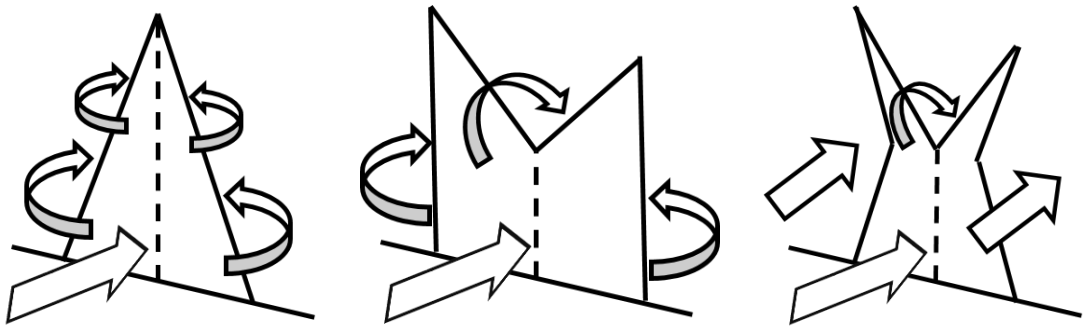

(a) **(b)** **(c)**

Fig. 6.11 Vortices in different VGs

6.5.4 Thermal Enhancement factor

Fig. 6.12 shows the variation of TEF for different conditions. The impact of different ambient conditions (varying ambient heat transfer coefficient) has been studied in Fig. 6.12 (a-c). Three different configurations of VGs have been investigated for their heat transfer capabilities in comparison to that of a smooth rectangular channel. In Fig. 6.12 (a-c), the horizontal dashed line depicts the TEF for a smooth channel which always acquires the value of 1. From Figs. 6.12 (a-c), it can be easily observed that the TEF increases consecutively for computational domains. The parameter exhibits greater than 1 value for all the computational domains except the first one. The obvious explanation for this is high pressure drop which occurs as a result of the first-time interaction of air with an obstruction in the form of a vortex generator. Subsequently, the Nusselt number upsurges while the pressure drop dwindles. The TEF increases by 2.54, 2.61, and 2.65 times for DVG, MVG, and FVG, respectively, from inlet to outlet at h=25W/m^{2}K. For h=15W/m^{2}K, the gains in TEF are 2.22, 2.91, and 2.32 for DVG, MVG, and FVG, respectively. The parameter value for the ambient condition of h=5W/m^{2}K mounts up by 1.7, 1.76, and 1.61 times for DVG, MVG, and FVG, respectively. The reasons behind this increment are turbulence enhancement, heat mixing, convection augmentation, and delayed boundary layer separation. Enhanced turbulence results in more efficient heat transfer by diminishing the thermal boundary layer and increasing the heat transfer coefficient. The vortices generated by vortex generators induce the mixing of the fluid, bringing hotter fluid from the core of the channel closer to the channel walls and vice versa. This mixing helps distribute heat more evenly across the channel cross-section, reducing the occurrence of hot spots and promoting more effective heat transfer. By increasing fluid motion and mixing, vortex generators enhance convective heat transfer, leading to improved heat dissipation from the channel walls. Furthermore, boundary layer

separation can lead to reduced heat transfer effectiveness. By delaying separation, vortex generators ensure that the flow remains attached to the channel wall for longer, maximizing heat transfer. The highest values are exhibited by the FVG incorporated channel, which are 3.278, 3.011, and 2.614 for h=25, 15, and 5W/m^{2}K, respectively.

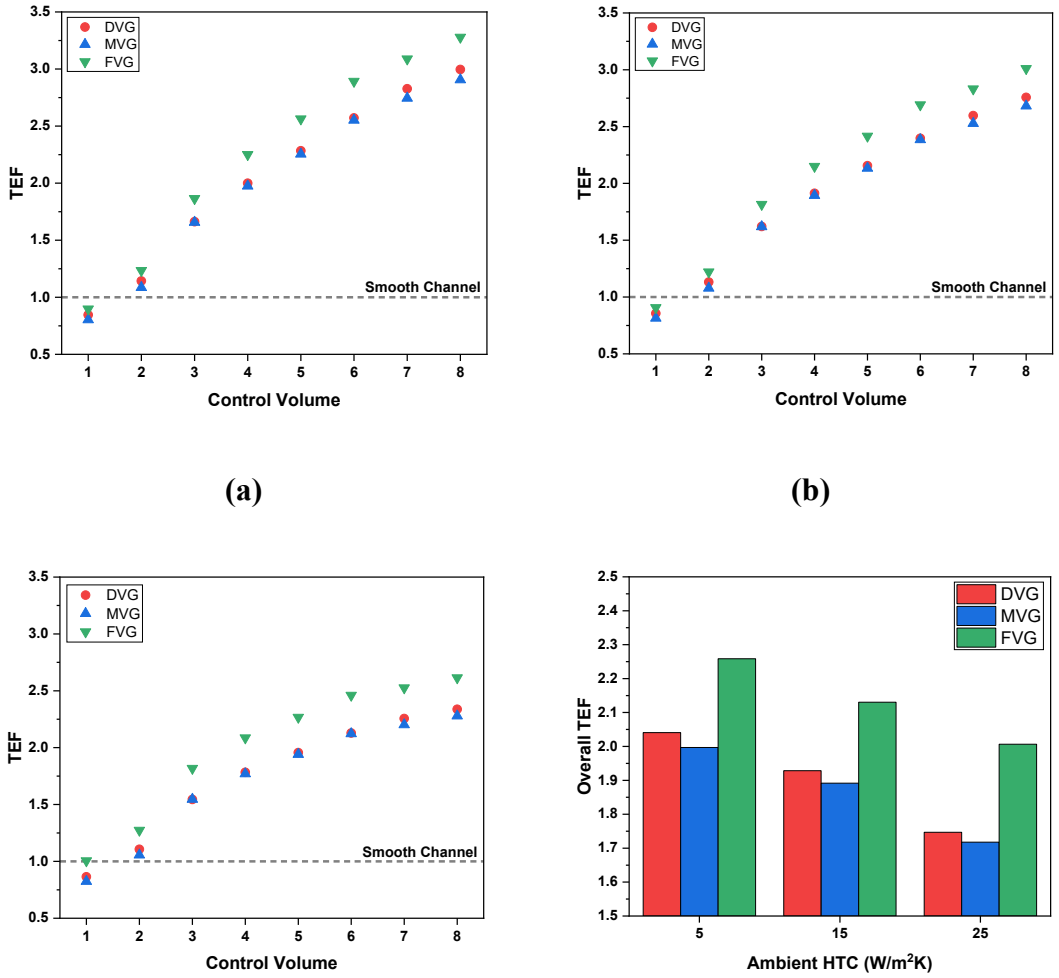

Fig. 6.12 Variation of (a) TEF in computational domains for h=25W/m^{2}K, (b) h=15W/m^{2}K, (c) h=5W/m^{2}K, and (d) Average TEF for different ambient conditions

Fig. 6.12 (d) shows the overall TEF across the channel. For h=25W/m^{2}K, the average TEF for DVG, MVG, and FVG incorporated channels are 104.1%, 99.69%, and 125.8% higher than that of the smooth channel. When the ambient condition is

studied at h=15W/m^{2}K, this increment is found to be 192.28%, 127.07%, and 153.18% for DVG, MVG, and FVG respectively. Furthermore, the parameter value increases by 121.51%, 108.14%, and 140.33% for DVG, MVG, and FVG respectively, against the smooth channel for h=5W/m^{2}K.

6.5.5 S/N ratio analysis

In the current study, the TEF (thermal enhancement factor) has been identified as the key factor as it incorporates both thermal and frictional aspects of the fluid flow. The optimization aimed to achieve the highest value of TEF. The optimization design uses L_9 orthogonal array which is described in Table 6.3.

Table 6.3: Designed L_9 orthogonal array (3^2) and the resulting TEF and S/N ratio values

Run	Factor		TEF	S/N
	A	B		
1	D	5	2.041	6.197
2	D	15	1.928	5.702
3	D	25	1.747	4.846
4	M	5	1.997	6.007
5	M	15	1.892	5.538
6	M	25	1.718	4.7
7	F	5	2.258	7.074
8	F	15	2.130	6.568
9	F	25	2.006	6.047

The S/N ratio values obtained after the utilization of the Taguchi method of the combinations obtained from the design of experiments are shown in Fig. 6.13. A higher value of the S/N ratio depicts more sensitivity of the objective function to that factor. The highest value of signal-to-noise ratio is exhibited by the factors A3 (fishtail VG), and B1 ($h=5W/m^2K$) out of the 9 runs. Table 6.4 shows the mean S/N ratio values as well as the rank obtained by the factors. It ranks the shape of the VG as first and the ambient HTC as second. This means that the shape of the VG had a greater influence on the thermohydraulic performance of the channel. However, if closely observed, the mean values obtained by the shape of the VGs are very close to that of the ambient HTC. This means, that even though the shape of the VGs stands first to the ambient HTC, the latter is as effective a factor as the former.

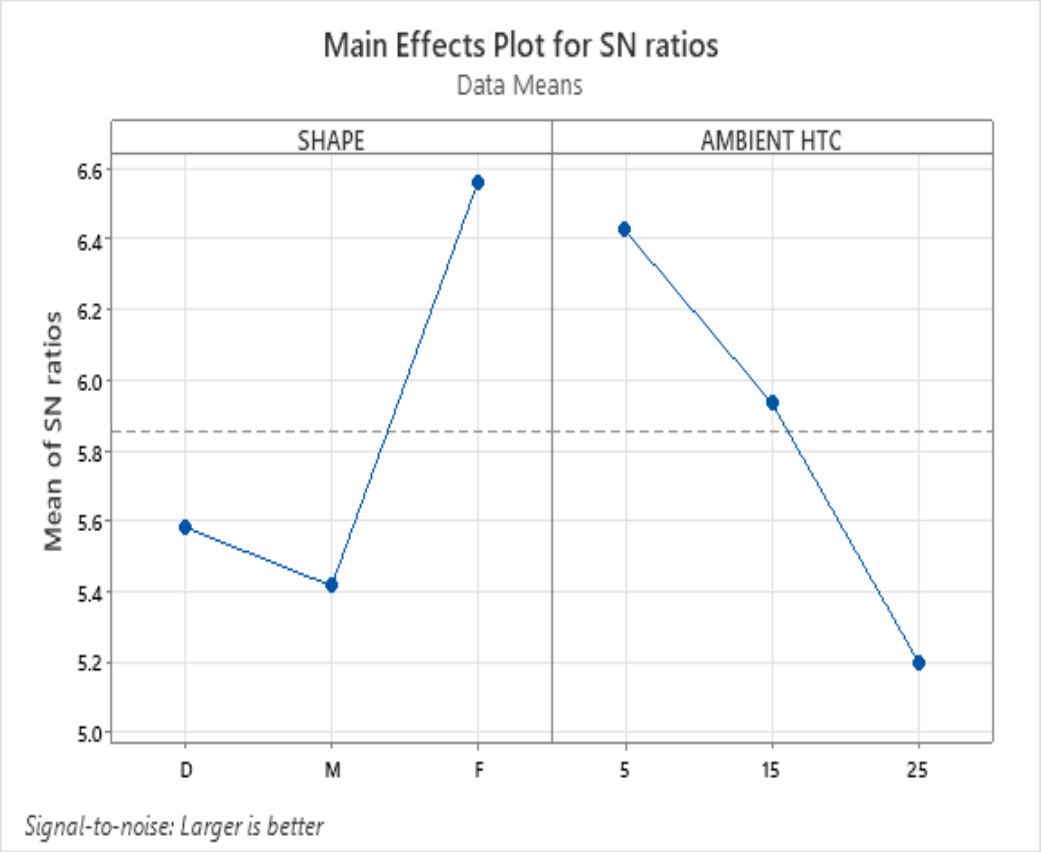

Fig. 6.13 SN ratios plot

Table 6.4: Response Table: for Signal-to-Noise Ratios

Criteria: Larger is better		
Level	**Shape**	**Ambient HTC**
1	5.582	6.426
2	5.415	5.936
3	6.563	5.198
Rank	**1**	**2**

Table 6.5: Analysis of Variance for SN Ratios

Source	DF	Seq SS	Adj SS	Adj MS	F	P
SHAPE	2	2.30706	2.30706	1.15353	103.87	0.003
AMBIENT HTC	2	2.29517	2.29517	1.14759	103.34	0.008
Residual Error	4	0.04442	0.04442	0.01111	-	-
Total	8	4.64666	-	-	-	-

In ANOVA (Analysis of Variance), the same can be predicted with the help of p-values. A small p-value (typically less than 0.05) implies that the observed differences in the means are likely not due to random chance alone, providing evidence in favor of the alternative hypothesis. In the context of the Taguchi method, this suggests that the factors being studied have a significant effect on the response variable. Table 6.5 exhibits that both factors acquire a value less than 0.05, implying that both parameters are critical to the performance of the channel. However, a smaller value means the greater influence of that factor, which again is owned by the shape of the VG.

6.5.6 Artificial Neural Network (ANN) model

In the current study, a two-layer feedforward network with sigmoid hidden neurons (with layer size 20) has been deployed (Fig. 6.14). To improve the predictability of the ANN model, the level of Factor B in the Taguchi method is increased from 3 to 21 levels in which the number of cases becomes 63 (=3x21). The range of the factor B remains the same but the values are taken at the interval of 1 i.e., 5,6,7…25W/m^{2}K. For the present ANN model, the data ratio used is 70:15:15 for training, validation, and testing. Thus, the overall model comprises of input, two hidden layers, and the output. The hidden layer used a sigmoid function for stimulation.

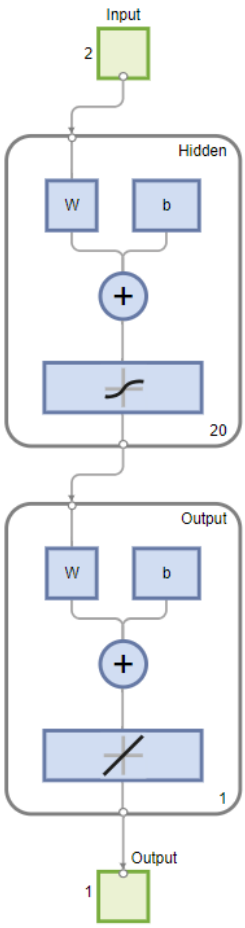

Fig. 6.14 Neural network visualization

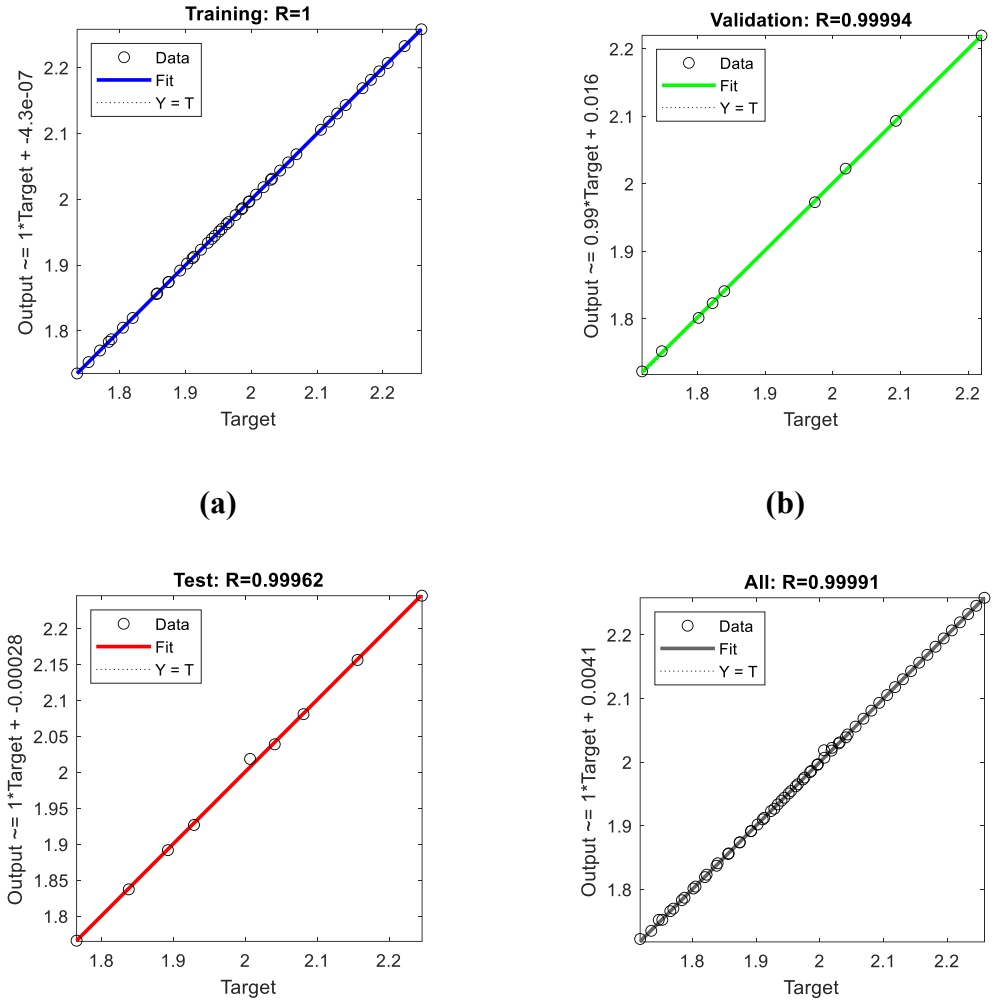

Fig. 6.15 (a-d) Prediction by ANN model for training, validation, and testing

The data division was taken randomly and the Levenberg-Marquardt training algorithm has been used along with mean-squared error performance. With 20 neurons in the hidden layer and 1 in the output layer, predicting fit quality (R^2) of 1, 0.99994, and 0.99962 (Figs. 6.15(a-d)). Hence, the present model configuration has very high prediction efficiency and can be used for similar computational problems.

6.6 Highlights

This work is aimed at numerically studying different geometries of vortex generators under different ambient conditions to ascertain the thermohydraulic

effectiveness of the VGs and carry out a comparative analysis. Various thermal and fluid flow parameters have been taken into consideration. Taguchi design-of-experiments is used to carry out the combinations of runs required for the analysis. The analysis of variance (ANOVA) and S/N ratios further helps in determining the optimum or the best factors for the outcome. Some salient features of the study are:

- Quantitatively, the heat transfer coefficient value at the outlet increases by 2.797, 2.777, and 2.834 times for DVG, MVG, and FVG respectively as compared to the inlet for h=25W/m^2K. Similarly, for h=15 W/m^2K, h raises by 2.801, 2.783, and 2.838 times at the outlet when compared to the parameter value at the inlet. For h=5W/m^2K, these values are 2.785, 2.766, and 2.566 for DVG, MVG, and FVG respectively.
- Out of all these, the maximum heat transfer coefficient is exhibited by FVG with a value of 554.17 W/m^2K for h=5W/m^2K.
- The pressure drops by 84.94%, 92.42%, 91.39%, and 89.44% for the smooth-, DVG-, MVG-, and FVG-incorporated channels.
- The highest TEF values are exhibited by the FVG incorporated channel, which are 2.258, 2.130, and 2.006 for h=25, 15, and 5W/m^2K, respectively.
- The highest value of signal-to-noise ratio is exhibited by the factors A3 (fishtail VG), and B1 (h=5 W/m^2K) out of the 9 runs.
- The machine learning ANN model gives the coefficient of determination value (R^2) of 1, 0.99994, and 0.99962 indicating high proficiency of the neural network.